Materials Science in Semiconductor Processing 37 (2015) 29–36

Contents lists available at ScienceDirect

Materials Science in Semiconductor Processing

journal homepage: www.elsevier.com/locate/mssp

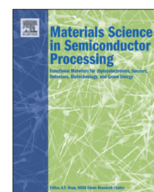

Influence of working pressure on the structural, optical and electrical properties of sputter deposited AZO thin films

Hyeongsik Park [a], S. Qamar Hussain [b], S. Velumani [a,c], Anh Huy Tuan Le [a], Shihyun Ahn [a], Sunbo Kim [b], Junsin Yi [a,*]

[a] College of Information and Communication Engineering, Sungkyunkwan University, Suwon 440746, Republic of Korea
[b] Department of Energy Science, Sungkyunkwan University, Suwon 440746, Republic of Korea
[c] Department of Electrical Engineering-SEES, CINVESTAV-IPN, Col San Pedro Zacatenco, D.F., Mexico C.P 07360, Mexico

ARTICLE INFO

Available online 2 February 2015

Keywords:
Zinc oxide
Thermal annealing
Mechanism
Thin film solar cell

ABSTRACT

Highly oriented crystalline aluminum doped zinc oxide (AZO) films were sputter deposited on glass substrates and a systematic investigation on the as deposited and etched films was reported for its further application in silicon thin film solar cell. Influence of the deposition pressure (from 2 to 8 mTorr) and post-annealing temperature (at 400 °C for 5 min) on the structural, optical and electrical properties of the as-deposited and etched samples were analyzed. The optimum condition for its reproducibility and large area deposition is determined and found that the depositions made at 8 mTorr at 200 W having the distance from source to substrate of 9 cm. All the AZO films exhibited a *c*-axis preferred orientation perpendicular to the substrate and their crystallinity was improved after annealing. From the XRD pattern the grain size, stress and strain of the films were evaluated and there is no drastic variation. Optical transmittance, resistivity, Hall mobility and carrier concentration for the as deposited and etched-annealed films were found to improve from 79 to 82%; 2.97 to 3.14×10^{-4} Ω cm; 25 to 38 cm^2/V s; 8.39 to 5.96×10^{20}/cm^3 respectively. Based on the triangle diagram between figure of merit and Hall mobility, we obtained a balance of point between the electrical and optical properties to select the deposition condition of film for device application.

© 2015 Elsevier Ltd. All rights reserved.

1. Introduction

Photovoltaic (PV) energy conversion is a key approach towards sustainability of humanity and conservation of valuable natural resources [1]. The improvement of both crystalline silicon and thin film solar cells has therefore attracted great interest over the last decade. Especially thin film solar cells offer a large potential for cost reduction and mass fabrication, however still there is great deficiency in energy conversion efficiencies as compared to other technologies. The introduction of thin transparent conductive layers of rough ZnO as a front contact and as a part of the back reflector in Si thin film solar cells can significantly reduce this drawback [2]. Aluminum (Al) or alumina (Al_2O_3) doped ZnO (AZO) has drawn much attention in PV devices, because they act as electrodes, structural templates, diffusion barriers, and their work function contributes to improve the open-circuit voltage. In short, from the cost, availability and environmental points of view, AZO appears to be a best candidate [3].

The physical properties of AZO films are generally dependent on deposition techniques and conditions. Many deposition techniques have been developed in order to obtain transparent and conductive AZO thin films, including magnetron

* Corresponding author.
E-mail addresses: richspark@skku.edu (H. Park), yi@skku.ac.kr (J. Yi).

http://dx.doi.org/10.1016/j.mssp.2014.12.076
1369-8001/© 2015 Elsevier Ltd. All rights reserved.

sputtering [4], pulsed laser deposition (PLD) [5], chemical vapor deposition (CVD) [6], spray pyrolysis [7], sol–gel process [8] and atomic layer deposition (ALD) [9]. Amongst them direct current (DC) magnetron sputtering is mostly used for large-area manufacturing in the thin film PV industry for mass production [10].

In addition, surface-textured AZO films with incident light-capturing ability have become an important issue to improve the photovoltaic efficiency for amorphous silicon (a-Si)/microcrystalline silicon (μc-Si) tandem solar cells (E_{ff}: 10.2% as the case of silicon thin film solar cell) [11,12]. For a-Si:H and μc-Si:H solar cells, relatively low optical absorption coefficients in the red and near-IR spectral ranges have been observed because of the indirect-transition nature of elemental silicon. A textured rough surface of the AZO layers can improve the performance by allowing efficient light scattering inside the solar cell and hence, more light absorption along the longer scattering path. Therefore, surface-texture techniques have received much interest and are becoming an industrial practice in the production of a-Si/nanocrystalline (nc-Si) and μc-Si solar cells.

The importance of the surface textured AZO films is to overcome the complicated contact between the AZO and p-type silicon layer [13]. The a-Si:H solar cells were fabricated with a p-μc-Si:H layer between the AZO and p-type amorphous silicon carbide (a-SiC:H) layers in order to reduce the surface potential barrier [14]. The improved photovoltaic properties are attributed to the reduction of surface barrier potential at the AZO/p-type contact layer [15]. By controlling the surface barrier potential, we can maximize the AZO/p-type layer contact properties. We investigated various samples like as-deposited, deposited-annealed, etched and etched-annealed, for reducing the surface potential barrier so as to improve electrical properties for AZO/p-type layer contact. In the present study, we sputter deposited AZO films at various working pressures and carried out surface morphological, optical and electrical properties. In order to get good haze ratio, all the films were etched with dilute HCl 0.5% solution for 35 s. Systematic investigations on the surface morphological, optical, electrical properties were carried out. Based on the triangle fitting between figure of merit and Hall mobility, we obtained a balance of point between the electrical and optical properties to select the deposition condition of film for device application.

2. Experimental

AZO films were deposited on Corning eagle glass substrates by radio frequency (RF) magnetron sputtering with 2 wt% Al_2O_3 doped ZnO target using the SNTEK, 09SN69 vacuum sputtering system. Prior to the deposition, the substrates were cleaned ultrasonically in acetone and isopropyl alcohol for 10 min, rinsed with deionized water, and dried in N_2 gas. Pre-sputtering of the AZO target was done for 5 min to remove the surface contaminants, before the film deposition. Power and angular speed of the substrate were fixed at 200 W and 5 rpm, respectively. The gas flow rate was fixed at 20 sccm and the working pressure was varied from 2 to 8 mTorr, keeping the substrate temperature at 200 °C for all the films. Later AZO films were textured by etching with dilute HCl (0.5%) solution for 35 s and then annealed at 400 °C. During the annealing process, the ramping rate of the temperature was kept at 3 °C/s.

The structural properties of the as deposited and etched-annealed samples were measured by a X-ray diffractometer (D8 Advance, Bruker) using Cu-Kα radiation. The surface morphology of the films was analyzed using a atomic force microscope (AFM), SPA-300 HV from SII, Japan. The thicknesses of the AZO films were measured

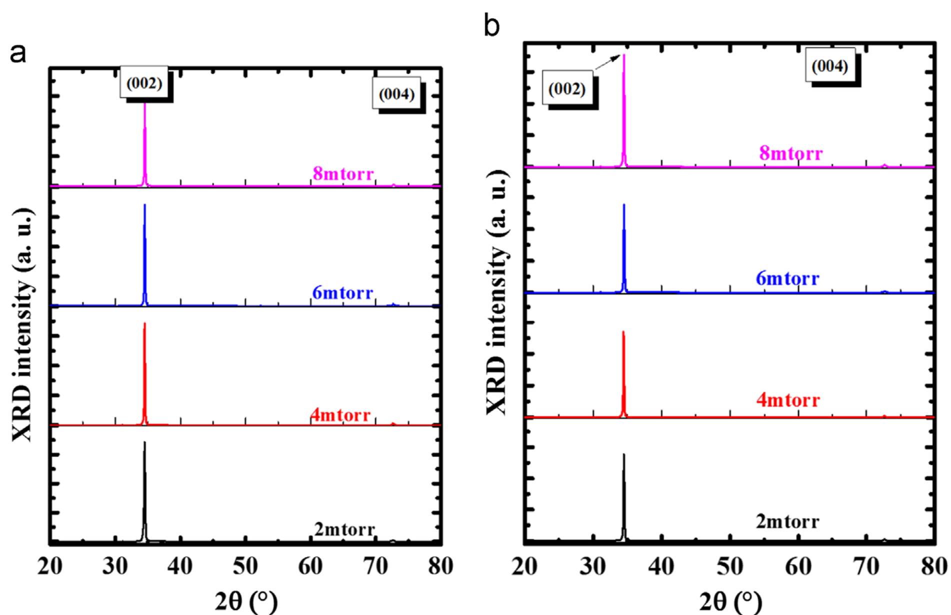

Fig. 1. XRD patterns of as-deposited and annealed (at 400 °C) AZO films at various working pressures. (a) as-deposited, and (b) annealed at 400 °C.

using a surface profiler (model: Tencor D-100) and a ellipsometry (model: SE MF-1000).

The grain sizes of the films were evaluated using the following Scherrer equation [16]:

$$D = \frac{0.9\lambda}{\beta \cos \theta} \quad (1)$$

where β is FWHM and λ (0.154 nm) is X-ray wavelength. The strain ε_1 and ε_2 are evaluated from the following equations [17]:

$$\varepsilon_1 = \frac{(d_{film} - d_{bulk})}{d_{bulk}} \times 100 \quad (2)$$

$$\varepsilon_2 = -\frac{\varepsilon_1}{\gamma} \quad (3)$$

where d_{film} and d_{bulk} correspond to the d-value of film and bulk (2.603 Å) and γ is Poisson's ratio (γ=0.36 for ZnO). Film stress was calculated from the following equation:

$$\sigma_{stress} = \frac{233(c - c_0)}{c_0} \quad (4)$$

where c is the lattice parameter of c-axis (002) for ZnO:Al thin film, and c_0 is the lattice parameter of ZnO bulk film (5.2066 Å) [18].

The total and diffused transmittance of AZO films were estimated with the help of an integrating sphere (model: QEX10) by quantum efficiency (QE) system. After measuring T_{total} and diffuse transmittance ($T_{diffuse}$), the haze ratio ($T_{diffuse}/T_{total}$) was calculated [19].

The mobility, concentration of charge carriers in the AZO films were measured by the Hall Effect set up (model: ECOPIA HMS-3000) and the resistivity of the films were evaluated using the following formula [20]:

$$\rho = \frac{1}{n_e e \mu_e} = n_e e^2 \frac{\tau}{m_e^*} \quad (5)$$

The sheet resistance was evaluated by 4-point probe method. Figure of merit (FOM), as proposed by Haacke [21], was calculated from Eq. (6) below using the average transmittance (T) and R_{sheet}. FOM can provide information for comparing the inter relation between the optical and

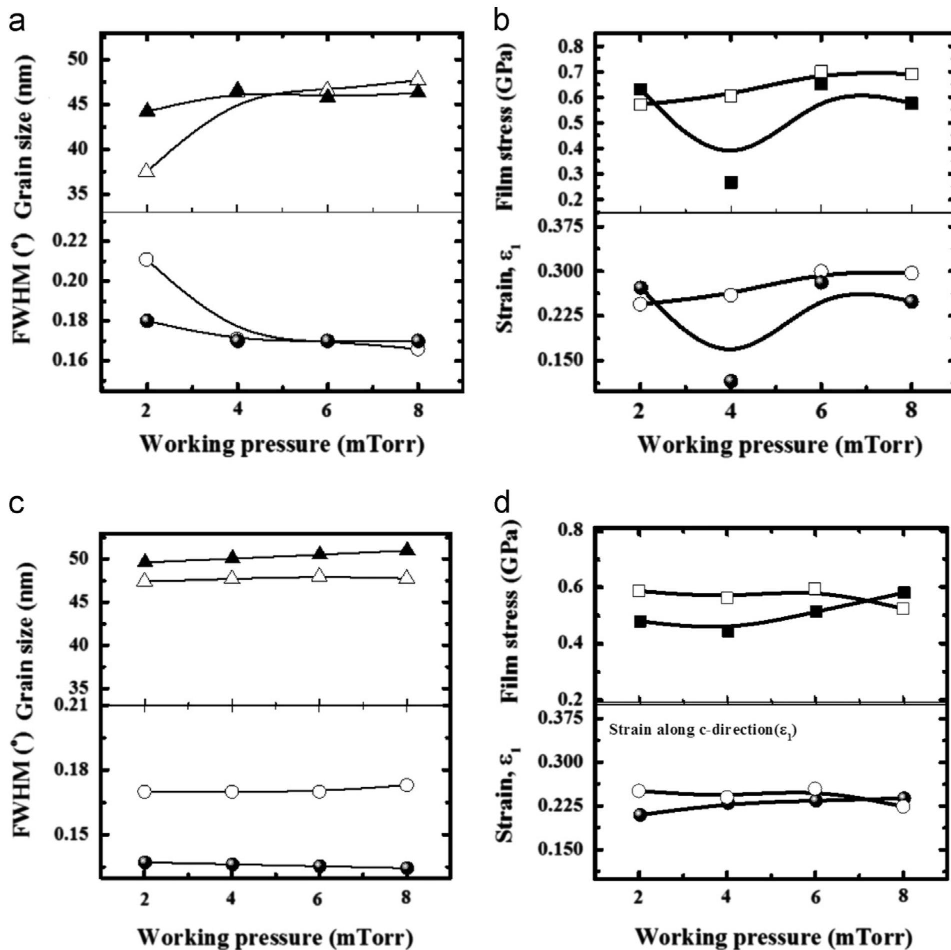

Fig. 2. The variation of (a) grain size, FWH and (b) Film stress, strain in the as-deposited (open type) and annealed at 400 °C (full type) as a function of working pressure. The variation of (c) grain size, FWHM and (d) Film stress, strain in the as-etched (open type) and etched-annealed (full type) as a function of working pressure.

electrical performance factor of the film.

$$FOM = \frac{T^{10}}{R_{sheet}} \tag{6}$$

3. Results and discussion

3.1. Properties of as deposited films

In this investigation, all the AZO thin films were deposited at RF power of 200 W, substrate temperature (T_s) of 200 °C varying working pressures from 2 to 8 mTorr with almost uniform thickness of 800 ± 5 nm. All the films were annealed at 400 °C in vacuum (10^{-3} Torr) for 5 min. Fig. 1 shows the plot of XRD and crystalline structures of as deposited and annealed films. All the samples showed intense (002) peaks corresponding to the diffraction at 34.5° and 72.5° corresponding to (004), indicating wurtzite structure [22]. The peak intensities of the annealed samples on the glass substrates were stronger than as-deposited ones [23–25]

Fig. 2(a) and (b) shows the variation of grain size, FWHM, stress and strain in the as-deposited and annealed films as a function of working pressure. Grain size was found to vary slightly for unannealed films and after annealing, it is found to be consistent around 46 nm. FWHM was minimum for the films deposited at 8 mTorr as compared to 2 mTorr, thus reflecting the high crystallinity of the structures. The stress and strain in the films does not depend upon the working pressure which depicts a variation of around ±5 either for, as deposited or annealed films. FWHM of the deposited films were 0.17 and other authors have reported higher values of around 0.447, which indicates larger grains. This reflects the improvement in the grain size in our deposition conditions leading to good conductivity and transportation of electrons [26,27].

Fig. 3(a)–(c) shows the surface roughness of the as deposited and annealed films. It is found that the RMS roughness of the annealed films decreases to 2.877 nm, thus indicating smoothness of the surface after annealing. This smoothening will not be useful for our application of light scattering in our Silicon based solar cells [28]. Therefore, in the next section we will deal with the etching process and further annealing. Fig. 3(a) and (b) displays the surface morphology of the as deposited and annealed AZO films over an area of 2 × 2 μm^2. The RMS value of annealed films decreased to 2.87 nm from 4.36 nm (unannealed) which indicates that there is no adsorption of O_2 or any other impurities on the surface [29].

Fig. 4(a) and (b) indicates the transmittance and reflectance of the as deposited and annealed AZO films deposited at various working pressures. The overall transmittance of the films improved after annealing. The haze evaluated from the ratio of diffused transmittance to the total transmittance, is found to be almost null due to smoothening of the surface [30].

Fig. 5 shows the variation of Hall mobility, carrier concentration and resistivity as a function of $P_{working}$ (as-deposited and annealed). The resistivity and mobility of the as-deposited films initially decreases with the increase in $P_{working}$ and tends to become constant. A minimum resistivity and mobility values are 2.98 × 10^{-4} Ω cm and 25 cm^2/V s respectively, for

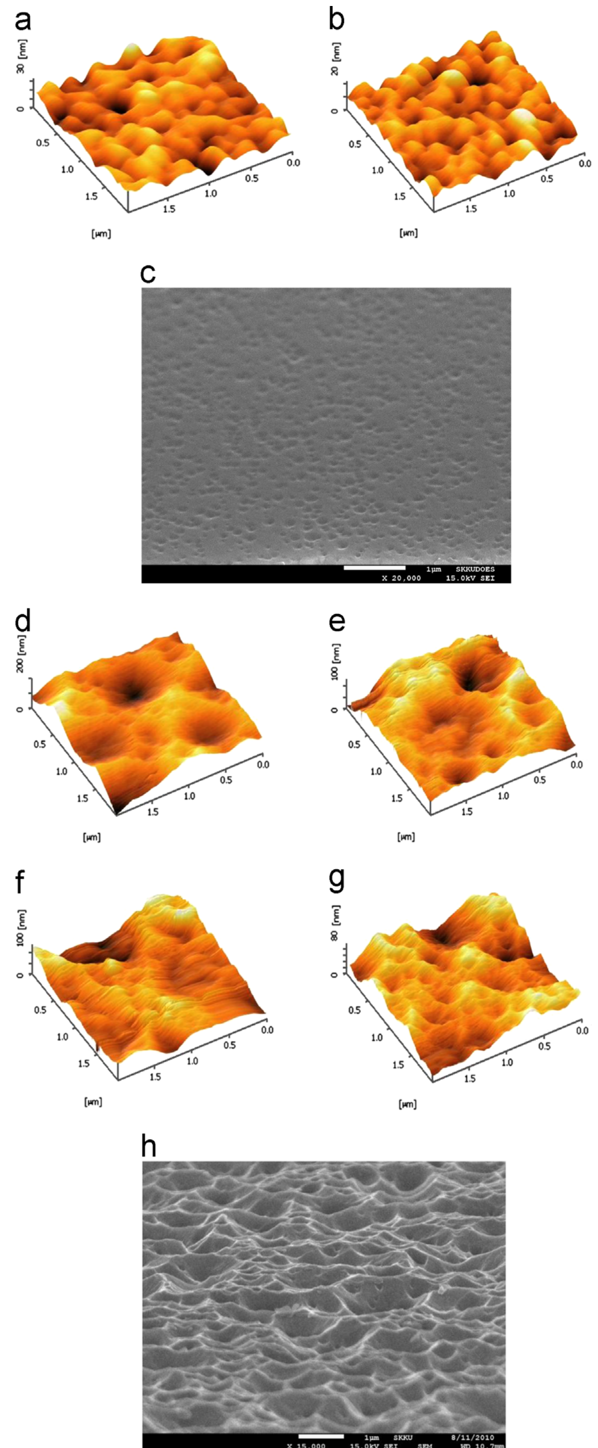

Fig. 3. Surface roughness of the as-deposited and annealed films from AFM image (a,b), FE-SEM image of as-deposited film (c). AFM images of etched-annealed at various working pressure; (d) 2 mTorr, (e) 4 mTorr, (f) 6 mTorr, (g) 8 mTorr. (h) FE-SEM image of as-etch sample at 2 mTorr. (a) RMS: 4.365 nm (as-deposited), (b) RMS: 2.877 nm (annealed), (c) as-deposited (2 mTorr), (Etched-annealed samples), (d) RMS: 28.7 nm (2 mTorr), (e) RMS: 22.48 nm (4 mTorr), (f) RMS: 21.44 nm (6 mTorr), (g) RMS: 17.63 nm (8 mTorr), and (h) as-etched (2 mTorr).

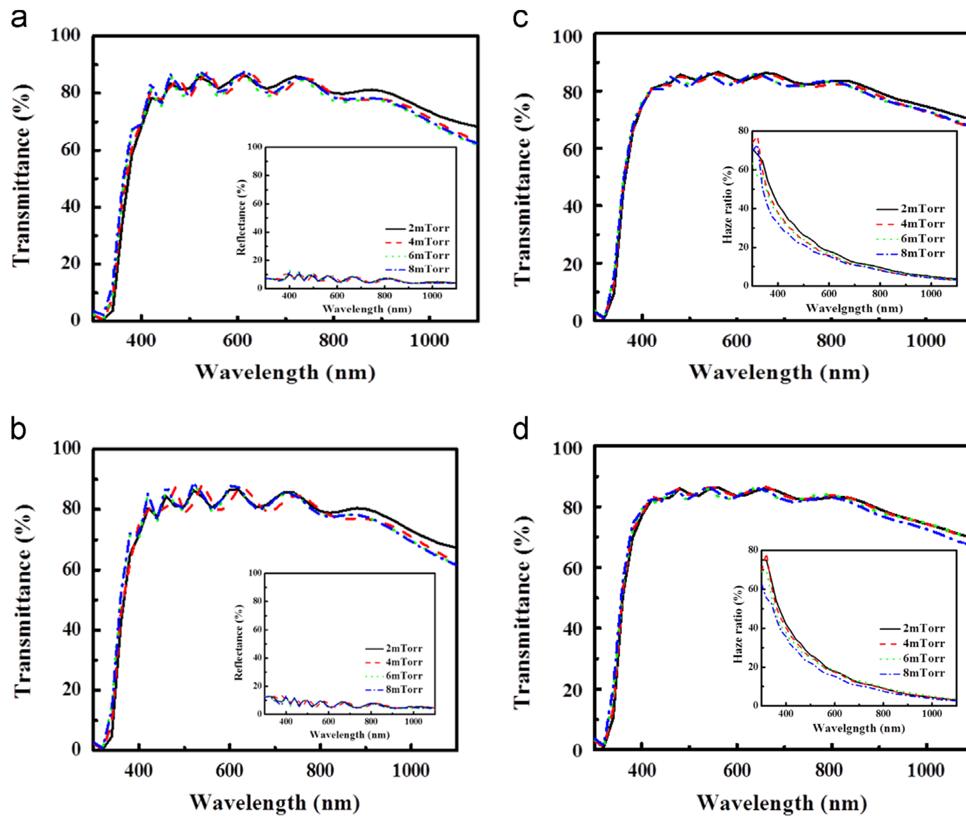

Fig. 4. Optical transmittance of (a) the as-deposited and (b) annealed films as a function of working pressure. (Inset graph: reflectance). (c) as-etched and (d) etched-annealed films as a function of working pressure. (Inset graph: Haze ratio), (a) as-deposited, (b) annealed at 400 °C, (c) as-etched, and (d) etched-annealed.

the films deposited at 8 mTorr. On the contrary, the carrier concentration decreased from $8.39\times10^{20}\,cm^{-3}$ (as-deposited) to $5.1\times10^{20}\,cm^{-3}$ (annealed) at 8 mTorr. These different behaviors could be explained by the desorption of oxygen in the grain boundaries which act as traps for the carriers. This leads to the decrease in the carrier concentration when the annealing process is performed in an ambient atmosphere, related to the number of electrons, electrons formed by the ionization of the interstitial zinc and the oxygen vacancies will affect the electrical conductivity [31,32].

It is evident that the R_{sheet} decrease from 6.17 to 4.07 Ω/sq without annealing and decrease from 5.78 to 3.96 Ω/sq with annealing as the $P_{working}$ increased from 2 to 8 mTorr. There was a significant increase in carrier concentration at various working pressures and was found to lie between $3.59\times10^{20}\,cm^{-3}$ and $8.39\times10^{20}\,cm^{-3}$, for as-deposited AZO samples. There was no significant increase in carrier concentration after annealing, which was around $5-7\times10^{20}\,cm^{-3}$. The Hall mobility of the as-deposited films exhibited a maximum value at about 2 mTorr and was found to be 37.5 cm^2/V s. The reason for the lower resistivity and higher Hall mobility at lower pressure can be explained by less collision among sputtered atoms and argon ions, thus leading to less energy loss [33].

3.2. Properties of etched and etched-annealed films

The annealed films discussed in the previous section had a very smooth surface morphology, which is not useful for our application to solar cells. Hence, we proceeded to etch the surface to have a rough surface morphology in order to trap and internally reflect the light effectively at the interface of AZO and a-Si. Etching of films were performed with dilute HCl (0.5%) solution for 35 s and then annealed at 400 °C. We report here the structural, morphological, optical and electrical properties of the etched and etched-annealed films. During the annealing process, the ramping rate of the temperature was kept at 3 °C/s.

As shown in Fig. 2(c), the FWHM of (0002) diffraction peak of the etched and etched-annealed samples decreased from 0.17 to 0.15, which indicates that the etched and etched-annealed sample had less stress and film strain due to the recrystallization after annealing. It can be observed that the grain size increased after annealing for all the films irrespective of deposition pressure. From Fig. 2(d) stress and the strain of the films decreases after annealing irrespective of working pressure but increases with working pressure. At 8 mTorr, the stress and strain of the etched-annealed films are found to be slightly greater than the as-etched samples due to the possible effect of the thermal stress [29].

The surface morphology (from AFM) of the etched-annealed AZO films is shown in Fig. 3(d)–(g). The RMS surface roughness was found to decrease after annealing, thus indicating smoother surface after annealing. Etched annealed samples had a RMS roughness around 10 times higher than the as deposited films. This is evident from the SEM image (Fig. 3(c)) of as-deposited AZO film, revealing a very smooth surface nature which is not useful for the internal scattering of light. Fig. 3(h) shows SEM image of

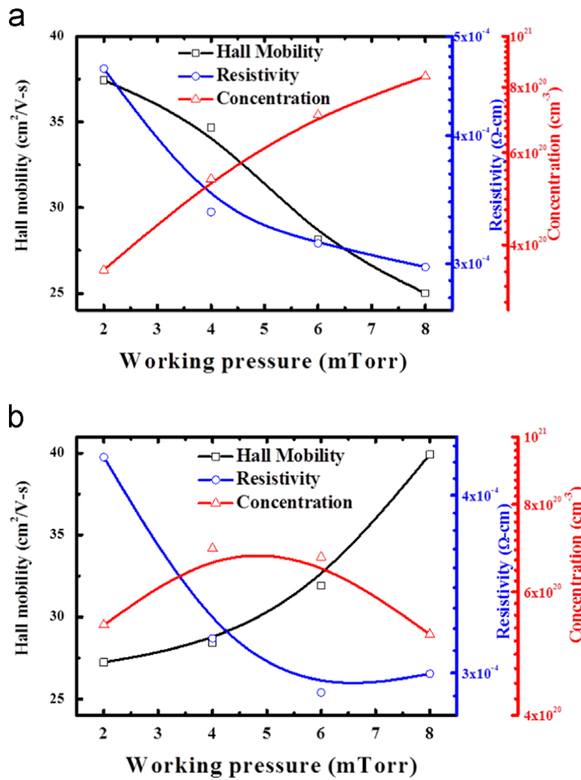

Fig. 5. Hall-Effect measurement of carrier concentration, resistivity and hall mobility of AZO films (a) as-deposited and (b) annealed on glass substrate at different working pressures, (a) as-deposited, and (b) annealed at 400 °C.

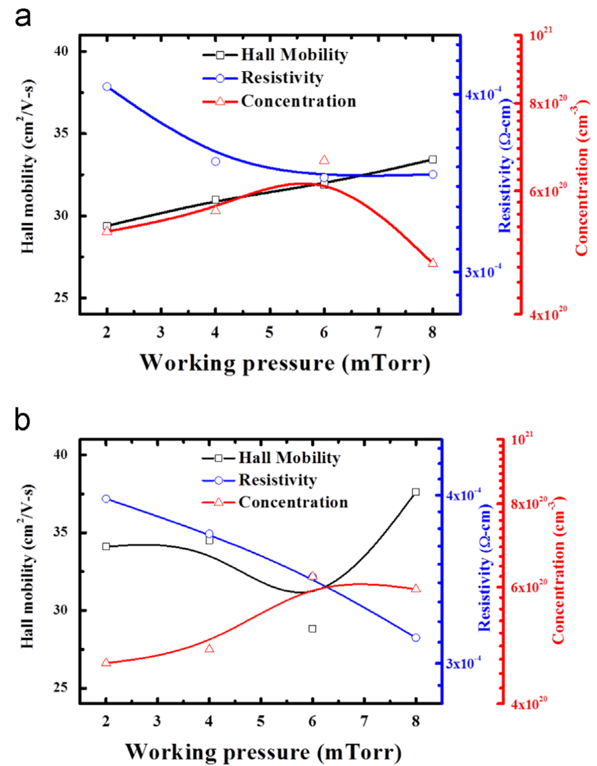

Fig. 6. Hall-Effect measurement of carrier concentration, resistivity and hall mobility of AZO films (a) etched with HCl 0.5% and (b) etched-annealed at different working pressures, (a) as-etched, and (b) etched-annealed.

as-etched AZO films. From these images, we can see that etching causes the surfaces to develop a lunar crater-like appearance with statistically spread flat craters [35]. The crater depths are found to decrease with increasing working pressure and subsequent decrease in RMS roughness, resulting in enhanced haze ratio for samples deposited at lower working pressure. Even though the higher surface roughness resulted in better light trapping effect, it had its consequences in the electrical properties. The higher crater-size surface morphology showed the high surface roughness and hence the high haze ratio as observed by various authors [36,37].

Optical properties are one of the vital factors determining the behavior of the incident light on the AZO surface, which can effectively guide it through the solar cells. Since our objective is to have the maximum internal reflection at the AZO/a-Si interface, rougher the surface, more is the internal reflections. But there should be good transmittance and higher conductivity. Fig. 4(c) and (d) shows the transmittance of the etched and etched-annealed samples, and in the inset a plot of the haze ratio as a function of wavelength at various working pressures. There is no significant change in the transmittance of the etched and etched-annealed samples, but overall the transmittance decreased after annealing [38]. Further, the transmittance decreased with increasing working pressure i.e. the transmittance of about 84.4% in the wavelength of 500 nm at the working pressure of 2 mTorr. With the increase in the working pressure from 2 to 8 mTorr, the transmittance decreased to 81.3%.

After measuring T_{total} and diffuse transmittance ($T_{diffuse}$) as described above, the haze ratio ($T_{diffuse}/T_{total}$) was calculated. The haze ratio provides an index for the characteristic of light scattering in the etched AZO film. The haze ratio is found to decrease with increasing working pressure in accordance with the surface morphology. The increase in haze ratio may be related to the higher surface roughness of textured AZO films [34,36–37]. Even though from the previous section (structural) and optical properties, the films deposited at lower working pressure are more favorable, but from the electrical properties, the higher working pressure yielded better electrical properties.

The electrical characteristics like resistivity, carrier concentration and Hall mobility of etched and etched-annealed films at various working pressure are shown in Fig. 6(a) and (b). The resistivity and carrier concentration of the etched and etched-annealed films decreased with increasing working pressure whereas the Hall mobility increased with increasing working pressure. After annealing in vacuum at 400 °C the overall resistivity and carrier concentration decreased and the Hall mobility increased irrespective of working pressure, it might be the oxygen vacancies and the interstitial Zn metals created, which increases the carrier concentration [39]. As indicated in the previous section, after annealing, the crystallinity of the films improved and the grain size increases which influenced the increase in conductivity and Hall mobility [40] Table 1.

Table 1
The variation of the electrical properties (carrier concentration, Hall mobility and resistivity) and optical property (transmittance) in the as-deposited, annealed films, the as-etched and annealed films as a function of working pressure.

Condition	Pressure (mTorr)	Hall mobility (cm^2/V s)	Resistivity ($\times 10^{-4}$ Ω cm)	Carrier concentration ($\times 10^{20}$ cm^{-3})	$T_{400–800\ nm}$ (%)
As-deposited	2	37.5	4.65	3.59	82.2
	4	34.7	3.37	5.34	82
	6	28.1	3.14	7.07	81.1
	8	25	2.98	8.39	82.1
As-deposited → annealed	2	27.23	4.26	5.39	82.3
	4	28.41	3.17	6.92	82.2
	6	32	2.91	6.7	82.2
	8	40	2.99	5.22	82.6
As-etched	2	29.4	4.05	5.25	83.6
	4	31	3.59	5.62	83
	6	32	3.45	6.63	83
	8	33.4	3.51	4.73	82.8
As-etched → annealed	2	34.1	3.98	4.6	83.7
	4	34.5	3.74	4.83	84
	6	28.8	3.48	6.22	83.4
	8	37.6	3.14	5.96	83.5

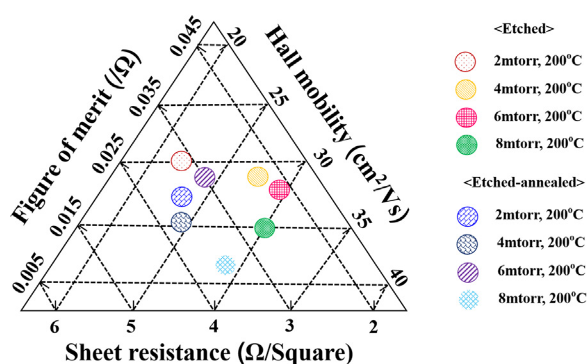

Fig. 7. Tri-angle diagram of etched and etched-annealed samples (figure of merit, sheet resistance and hall mobility).

Fig. 7 shows the triangular plot of sheet resistance (R_{sheet}), Hall mobility and figure of merit (FOM) for films deposited at various pressures. This plot will be useful to identify optimum parameters to obtain good quality films striking a balance between the optical and electrical properties with deposition condition. From the plot we can identify that at 8 mTorr the films had minimum sheet resistance, FOM and carrier concentration with higher mobility suitable for solar cell application.

4. Conclusion

There is a considerable influence of the working pressure on the electrical properties of the sputter deposited AZO films. With an increase in working pressure, the grain size increased and the stress and strain in the films decreased. Since the as deposited and annealed films does not yield good haze ratio values, all the films were etched using dilute HCl and further annealed. Even though the optical transmittance almost remained similar for the as deposited, etched and etched-annealed films, there is significant change in the haze ratio after etching and annealing. The optimum conditions for its reproducibility and large area deposition are determined and found that; the depositions made at 8 mTorr and 200 W having the distance from source to substrate of 9 cm. Based on the triangle fitting between figure of merit, resistivity and hall mobility, we obtained a balance of point between the electrical and optical properties to select the deposition conditions of the film for device application.

Acknowledgment

This work was supported by the Human Resources Development program (No. 20144030200580) of the Korea Institute of Energy Technology Evaluation and Planning (KETEP) grant funded by the Korea government Ministry of Trade, Industry and Energy.

References

[1] N.S. Lewis, Science 315 (2007) 798.
[2] M. Kubon, F. Boehmer, F. Siebke, B. Rech, C. Beneking, H. Wagner, Sol. Energy Mater. Sol. Cells 41–42 (1996) 485.
[3] W. Beyer, J. Hüpkes, H. Stiebig, Thin Solid Films 516 (2007) 147.
[4] L. Bai, B. Liu, J. Fan, D. Zhang, C. Wei, J. Sun, Y. Zhao, X. Zhang, J. Power Sources 266 (2014) 138.
[5] L. Moreno, C. Sánchez-Aké, M. Bizarro, Appl. Surf. Sci. 302 (2014) 46.
[6] T. Kobayashi, T. Nakada, Jpn. J. Appl. Phys. 53 (2014) 05FA03.
[7] T.G. Silva, E. Silveira, E. Ribeiro, K.D. Machado, N. Mattoso I.A. Hümmelgen, Thin Solid Films 551 (2014) 13.
[8] T. Ivanova, A. Harizanova, T. Koutzarova, B. Vertruyen, Mater. Lett. 64 (2010) 1147.
[9] D.J. Lee, H.M. Kim, J.Y. Kwon, H. Choi, S.H. Kim, K.B. Kim, Adv. Funct. Mater. 21 (2011) 448.
[10] L.-J. Meng, M.P. dos Santos, Thin Solid Films 250 (1994) 26.
[11] O. Kluth, B. Rech, L. Houben, S. Wieder, G. Schöpe, C. Beneking, H. Wagner, A. Löffl, H.W. Schock, Thin Solid Films 351 (1999) 247.
[12] J.C. Lee, V. Dutta, J. Yoo, J. Yi, J. Song, K.H. Yoon, Superlattices Microstruct. 42 (2007) 369.
[13] S. Gall, C. Becker, E. Conrad, P. Dogan, F. Fenske, B. Gorka, K.Y. Lee, B. Rau, F. Ruske, B. Rech, Sol. Energy Mater. Sol. Cells 93 (2009) 1004.
[14] J.J. Park, V.A. Dao, C.H. Shin, H.S. Park, M.B. Kim, J.H. Jung, D.Y. Kim, J. Yi, Thin Solid Films 546 (2013) 331.
[15] J.E. Lee, J.H. Park, J.S. Cho, J.W. Chung, J. Song, D.W. Kim, J.C. Lee, Thin Solid Films 520 (2012) 6007.
[16] Z. Zhang, C. Bao., S. Ma, L. Zhang, S. Hou, J. Aust. Ceram. Soc. 48 (2012) 214.

[17] G.P. Daniel, V.B. Justinvictor, P.B. Nair, K. Joy, P. Koshy, P.V. Thomas, Phys. B 405 (2010) 1782.
[18] Y.-Y. Chen, P.W. Wang., J.-C. Hsu, C.-Y. Lee, Vacuum 87 (2013) 227.
[19] Y.-J. Lee, H.S. Park, M.K. Ju, Y.K. Kim, J.J. Park, D.V. Ai, S.Q. Hussain, Y.S. Lee, S.H. Ahn, J. Yi, Energy 66 (2014) 20.
[20] B.Y. Oh, M.C. Jeong, D.S. Kim, W. Lee, J.M. Myoung, J. Cryst. Growth 281 (2005) 475.
[21] G. Haccke, J. Appl. Phys. 47 (1972) 1368.
[22] F.C.M. Van De Pol, F.R. Blom, Th. J.A. Popma, Thin Solid Films 204 (1991) 349.
[23] M.C. Jun, J.H. Koh, Nanoscale Res. Lett. 7 (2012) 294.
[24] H.J. Cho, S.U. Lee, B.Y. Hong, Y.D. Shin, J.Y. Ju, H.D. Kim, M.G. Park W.S. Choi, Thin Solid Films 518 (2010) 2941.
[25] H. Tong, Z. Deng, Z. Liu, C. Huang, J. Huang, H. Lan, C. Wang, Y. Cao, Appl. Surf. Sci. 257 (2011) 4906.
[26] Z.B. Fang, Z.J. Yan, Y.S. Tan, X.Q. Liu, Y.Y. Wang, Appl. Surf. Sci. 241 (2005) 303.
[27] M. Wang, J. Wang, W. Chen, Y. Cui, L. Wang, Mater. Chem. Phys. 97 (2006) 219.
[28] M.K. Puchert, P.Y. Timbrell, R.N. Lamb, J. Vac. Sci. Technol. A 14 (1996) 2220.
[29] M. Chen, Z.L. Pei, X. Wang, C. Sun, L.S. Wen, J. Vac. Sci. Technol. A 19 (2001) 963.
[30] S.J. Tark, M.G. Kang, S.G. Park, J.H. Jang, J.C. Lee, W.M. Kim, J.S. Lee D.H. Kim, Curr. Appl. Phys. 9 (2009) 1318.
[31] P. Nunes, E. Fortunato, R. Martins, Thin Solid Films 383 (2001) 277.
[32] S.Y. Kuo, W.C. Chen, F.-I. Lai, C.-P. Cheng, H.-C. Kuo, S.-C. Wang W.-F. Hsieh, J. Cryst. Growth 287 (2006) 78.
[33] L. Zhifang, C. Guangyu, G. Shibin, D. Lingling, Y. Rong, M. Yuan, G. Ted, L. Liwei, J, J. Semiconductors 34 (2013) 063004.
[34] X. Yana, S. Venkataraja, A.G. Aberle, Energy Procedia 33 (2013) 157.
[35] O. Kluth, G. Schope, J. Hüpkes, C. Agashe, J. Müller, B. Rech, Thin Solid Films 442 (2003) 80–85.
[36] Y.C. Lin, T.Y. Chen, L.C. Wang, S.Y. Lien, J. Electrochem. Soc. 159 (2012) H599.
[37] A. Hongsingthong, I.A. Yunaz, S. Miyajima, M. Konagai, Proceedings of the IEEE on Photovoltaic Specialists Conference (PVSC), 2010, 001508.
[38] S. Flickyngerova, M. Netrvalova, L. Prusakova, I. Novotny, P. Sutta, V. Tvarozek, Vacuum 84 (2010) 215.
[39] B.G. Choi, I.H. Kim, D.H. Kim, K.S. Lee, T.S. Lee, B. Cheong, Y.-J. Baik, W.M. Kim, J. Eur. Ceram. Soc. 25 (2005) 2161.
[40] K.-K. Kim, H. Tampo, J.-O. Song, T.-Y. Song, S.-J. Park, J.-M. Lee, S.-W. Kim, S. Fujita, S. Niki, Jpn. J. Appl. Phys. 44 (2005) 4776.